Indian Journal of Research in Applied Sciences Engineering (IJRASE)
Vol.2.No.1 2014pp 18-25.
available at: www.goniv.com
Paper Received :05-03-2014
Paper Published:28-03-2014
Paper Reviewed by: 1. John Arhter 2. Hendry Goyal
Editor : Prof. P.Muthukumar

SKIN LESION CLASSIFICATION USING HYBRID SPATIAL FEATURES AND GR NETWORK

Iswarya.M[1], Karpagam.R[2], Kausalya.M[3]
[1,2,3]P.S.R.Rengasamy College Of Engineering For Women,
Anna University, Chennai.

ABSTRACT

We present color image processing methods for the analysis of images of dermatological lesions. The focus of this study is on the application of feature extraction and selectionmethods for classification and analysis of the tissue composition of skin lesions or ulcers, in terms of granulation (red), fibrin (yellow), necrotic (black), callous (white), and mixed tissue composition. The images were analyzed and classified by an expert dermatologist into the classes mentioned previously. Indexing of the images was performed based on statistical texture features derived from cooccurrence matrices of the red, green, and blue (RGB), hue, saturation,and intensity (HSI), L*a*b*, and L*u*v* color components. Feature selection methods were applied using theWrapper algorithm with different classifiers. The performance of classification was measured in terms of the percentage of correctly classified images and the area under the receiver operating characteristic curve, with values of up to 73.8% and 0.82, respectively.

Index Terms—Color image processing, color texture, dermatologicalulcers, feature selection, machine learning, pattern recognition,tissue composition

I.INTRODUCTION

ULCERATION of the lower leg affects about 1% of the population, causing considerable morbidity[1]. Ulcers are usually caused by deficit in blood circulation and can be associated with arterial or venous insufficiency. Other causes are related to diabetes, vascular diseases, tumors, infection, and certain specific skin conditions. The healing process of an ulcer canbe divided into three phases: inflammation,tissue formation, and remodeling [2]. Inflammation is a protective response of the body, characterized by the activation of the immune system and redness of the affected tissue. After this step, tissue formation begins, with the formation of granulation tissue, which is the main component of most of capillaries and fibroblasts [3]. Finally,remodeling occurs with healing and reepithelialization

However, chronic wounds, such as venous ulcers, follow a more complex seesaw healing pattern [2]. Tissue injury is followed by the formation of a provisional matrix of fibrin that facilitates the influx of inflammatory and vascular endothelial cells during wound healing. Burnand *et al.* [4] showed that fibrin is present in ulcer-bearing skin and postulated that this accumulation within the tissue is the result of larger quantities of fibrinogen escaping through capillary pores, which are enlarged by the raised venous pressure. During the healing process, the skin can change to a transient phase of necrosis [5]. The existence of focal occlusions of arterioles in deep dermal plexus, small thrombi, and reduced vascular density suggests that necrosis develops as a result of vascular insufficiency [5]. In addition, callous is a hyperkeratotic lesion with a broad base and relatively uniform thickness which has lost its physiological function of protection, exacerbating the consequences of neuropathy, such as diminished pain perception [6]. Callous tissue is tough and hard, and thereby increases the already present pressure and contributes to more extensive lesions [7].

In dermatologic clinical routine, usually, medical professionals base the diagnosis of skin lesions mainly on visual assessment of pathological regions and evaluation of macroscopic features [8]. This fact indicates that correct diagnosis is highly dependent on the observer's experience and visual

perception[9]. The appearance of a wound, lesion, or ulcer provides important clues that can help with the diagnosis, determination of severity, and the prognosis of healing [10].

Quantification of the color and texture distribution of skin lesionsby image processing techniques could assist in the analysis of the dynamics of the underlying pathological processes as well as the progress of healing and response to treatment [9], [11].Inasmuch as automatic classification of ulcers is a relevant stage in computer-aided decision making [12], evaluation of the extractedfeatures in the image processing steps is important to determine which features, attributes, or measures are more descriptive or relevant than others. The major objective of this study is to evaluate several techniques of feature or attribute extraction and selection to determine which color and texture features are more useful in the classification of images of dermatological ulcers. This study is an expanded and updated version of a recent related conference presentation [12].

II. METHODOLOGY

A. Database of Images

A database consisting of 172 dermatologic images has beenprepared to date, obtained from outpatients at the University Medical Center, School of Medicine of Ribeir˜ao Preto, University of S˜ao Paulo, S˜ao Paulo, Brazil. Images included in database refer to venous and arterial insufficiency and diabetic wounds. The included wounds were located in different parts of inferiors members, with variable sizes. The skin color distribution among the subjects was predominantly white and only one lesion was included per patient. The age and gender distribution among the patients were not available due the patients' data anonymizing.

Approval was obtained from the Medical Center Ethics Committee for this research. Images were obtained based on a specific protocol that was determined after initial tests [13]. All images were obtained with the same digital camera (CanonEOS 5D0, 2 Megapixels), a 50-mm macro lens with a polarizing filter, and a circular flash; see Fig. 1 for examples of images of various types of ulcers. The typical size of the color images is 1747 × 1165 pixels with 24 b/pixel.

The tissue composition of each lesion was classified independently by an expert dermatologist (MACF), based on the color composition, as granulation (red), fibrin (yellow), necrotic (black), hyperkeratotic or callous (white), and mixed tissue. The dermatologist was blinded to the results of image processing. The 172 images in the database include 51 images of lesions
predominantly composed of granulation, 31 images of fibrin,three images of necrotic, three images of hyperkeratotic or callous, and 84 images of mixed tissue. The dermatologist also drew the boundaries of the lesions.

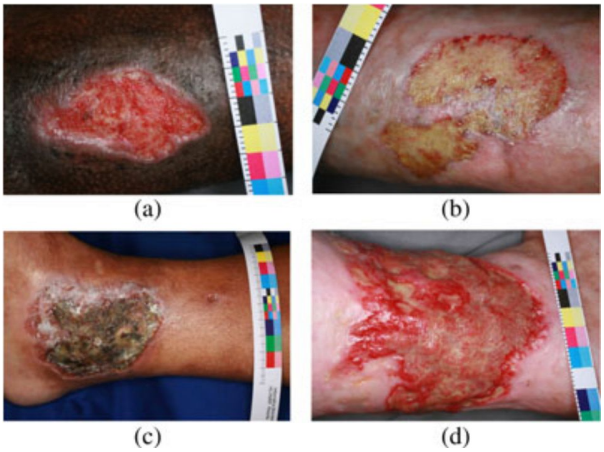

Fig. 1. Examples of images of various types of ulcers. (a) Granulation ulcer;
(b) fibrin ulcer; (c) necrotic ulcer; and (d) mixed-tissue ulcer.

A blue cloth was used to create a background in a color not expected to be present within the ulcer or on the part of the body being imaged, which was visible in most of the images. Color patches and rulers were included in the images (see Fig. 1) to facilitate color normalization and calibration of the images. A suite of color image processing, pattern analysis, and classification methods is being developed to facilitate image analysis.

B. Feature Extraction and Classification

Each image was independently and manually segmented into two regions representing the lesion and the background by an MACF. For each region representing a lesion, in addition to the basic RGB color components, six images were generated. According to t based on the hue (H) component and another was generated based on the saturation (S) component [15]. According to theL*u*v* color representation [14], [15], an image was generated based on the u* component and another was generated based on the v* component. Similarly, according to the L*a*b* color representation [14], [15], an image was generated based on the a* component and another was generated based on the b* component.

Values of the mean, standard deviation, skewness, and kurtosis were computed from the

histogram of each of the R, G, B, H, S, u*, v*, a*, and b* components. Also, the fivemost discriminative of the 14 texture features proposed by Haralick*et al.* [16] were derived from an averaged cooccurrence matrix (CoM) computed from four CoMs for a distance of one pixel at 0◦, 45◦, 90◦, and 135◦. The features are homogeneity, contrast,correlation, entropy, and local homogeneity, as suggested by Conners and Harlow [17], and were computed for each of the R, G, B, H, S, u*, v*, a*, and b* components. Furthermore, the five texture features mentioned earlier were computed from multispectral or color cooccurrence matrices (CCMs), obtained from the RG, GB, BR, HS, u*v*, and a*b* components, using the method proposed by Arvis *et al.* [18]. The method is an extension of the method of Haralick *et al.* [16], and was developed for application to color images to take into account the correlation existing between the color components, as shown in Fig. 2. Thus, a total of 111 features were extracted from the R, G, B, H, S, u*, v*, a*, and b* components to characterize each color image [12].

In the process of classification among the different types of skin ulcers, the extracted features should be evaluated to determine, which are more relevant to the solution of the problem[19]. The existence of correlated attributes in the set of features used can dramatically change the precision of certain classifiers. On the other hand, some classifiers lose precision due to the existence of more attributes than the desirable optimal set [20]. Thus, it is important to check the suitability and relevance of the available features in the context of the present problem [21]. The experiments described in this study were conducted using the open-source softwareWeka 3.6.4 [22]. The default values provided in Weka were used for all parametersof the feature selection and classification methods utilized in this study. Only the options for the number of folds in crossvalidation and the number of nearest neighbors were varied in the experiments.

From the algorithms available to perform attribute or feature selection, the Wrapper algorithm was chosen. The Wrapper algorithm generates candidate subsets of attributes and evaluates them by using a learning scheme [19]. This process is repeated with each candidate set until the stopping criterion is reached. Cross validation is used to estimate the accuracy of the learning scheme for a given set of attributes [19]. Cross validation is a sampling method for the analysis of the performance of a classifier that randomly divides the samples into r mutually exclusive partitions (folds) of approximately equal size of n/r samples, where n is the total number of available samples. The classifier is trained with the $r - 1$ induced folds of samples and the classification rule or methodology so derived is tested on the remaining fold. This process is repeated r times, so that each fold is used once as the test set. In this study, we have used fivefold cross validation

. The classifiers chosen to run the Wrapper algorithm are the Naive Bayes [23], multilayer perceptron (MLP) [24], decision tree [25], and *k*-nearest-neighbor (KNN) methods.The naive Bayes classifier calculates the probability of a sample belonging to each of the predetermined classes, assuming that there is independence between the attributes that describe the sample [23]. This probability value is used to generate a model with a decision rule that always provides a response indicating the class that has the highest probability after application of Bayes theorem .

The MLP classifier consists of a set of nodes that constitute the input layer, one or more intermediate or hidden layers of computational nodes, and an output layer [24]. The set of measurements to be classified is provided to the input layer and propagates forward, through the hidden layers toward the output layer, creating a computed value for classification.

Decision trees employ a strategy of divide-and-conquer, decomposing a larger problem recursively into simpler subproblems [25]. The construction of a tree is based on the choice of an attribute that will serve as a node to divide the samples into subsets according to the attribute value. The samples are analyzed for subsets according to the value of the respective attributes, and for each subset, it is verified if all of the samples belong to the same class. If this condition is satisfied, a leaf is created that selects the samples for the subset. The classification of a new sample starts from the root of the tree and proceeds through each decision node until arrival at a leaf . The class of the new sample is given by the class of the leaf[28]. The J48 implementation of decision trees was used in this study.

TheKNNclassifier finds the *k* nearest neighbors of the sample to be classified, typically by using a distance metric (usually the Euclidean distance) between the attributes of the sample to be classified and the attributes of all of the available samples with known classification [15]. In this study, the *k* value used for theKNN classifier is 10.

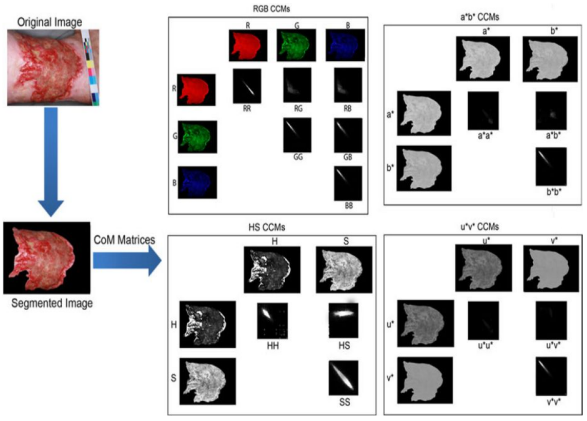

Fig. 2. Creation of CCMs for the analysis of texture in color images

C. Space Search Algorithms

The Wrapper algorithm needs to have a search engine. We used genetic search[29], greedy search (hill climbing) [19], and linear forward selection search [30].

Genetic search algorithms are implemented as a computer simulation in which a population of abstract representations of the solution is selected in search of better solutions [29]. The evolution usually starts from a set of randomly created solutions, and is carried through generations. In each generation, the adaptation of each solution is evaluated with the population; some individuals are selected for the next generation, and mutated or recombined to form a new population. The new population is then used as the input for the next iteration.

The hill-climbing search technique, also called greedy search or steepest ascent, is an algorithm that expands the current node and moves to the child node with the highest accuracy, terminating when no child node provides improvement over the current node [19].

Linear forward selection search takes a restricted number of l attributes into account. The search uses either the initial order of the attributes or a ranking that is performed to select the top *l* attributes. The search direction can be forward, or a floating forward selection approach could be used, and the procedure stops at a precomputed optimal size of the subset[30] .

D. Evaluation of the Results

Twelve feature selection tests were conducted, using all of the 111 features extracted for each image, with the four classifiers and the three search algorithms mentioned in Sections II-B and II-C, respectively. The selected attributes were stored and compared to verify which were selected more often.

We analyzed the frequency of selection of each attribute in the twelve tests. An evaluation test was conducted with the classifiers used (naive Bayes, MLP, KNN, and decision trees) and the attributes selected once or more, twice or more, until eight times, which was the highest frequency obtained. The labeling of the images by the dermatologist was used in training and testing of the classifiers. The percentage of correctly classified images and the area under the receiver operating characteristic (ROC) curve were computed for comparative analysis.

The ROC curve is obtained by plotting a graph of the sensitivity versus (1-specificity). The specificity of classification was computed in each experiment as the ratio of true positives to the number of positive samples. The sensitivity of classification is the ratio of the true negatives to the number of negative samples. Then, the area under the curve (AUC) is calculated. A large AUC indicates good performance in classification. In this study, due to the existence of five classes of ulcers, ROC analysis was performed in five steps, treating each class as positive and the remaining four classes as negative. A weighted average was then computed using the five AUC values so obtained.

III. RESULTS AND DISCUSSIONS

The frequency of selection of each feature is shown in Table I,separated by color space. The highest frequency of selection obtained in the experiments conductedwas 8. Only 22 of the 111 features were selected with one-half of the highest frequency or more often; among these features, 18 were derived from CCMs. Furthermore, only features from the L*a*b* and L*u*v* color spaces were selected more than four times, and all of them were features derived from CCMs.

Classification experiments were performed with all sets of attributes selected once to eight times. Fig. 3 shows the percentage of correctly classified images for each threshold on the frequency of selection of the attributes; the abscissa shows the number of features in each set. Fig. 4 shows the weighted average AUC for each experiment as described ealier.

The best classification with the naive Bayes classifier was obtained with only two features that were selected eight times each, with the correct classification rate of 73.3%. The two attributes selected eight times are the contrast between the components u*and v*, and the entropy between the components a* and b*.

When all of the 111 features were used, the MLP classifier provided the best classification accuracy of 70.4%, and AUC =0.75. Table II shows the confusion matrix for this case. We can observe

high performance in the classification of the fibrin and mixed categories, with accuracy up to 76%.

The best classification with the MLP was obtained using four attributes, which were the attributes selected six or more times, with an accuracy of 73.8% and AUC of 0.82. This was the highest classification accuracy obtained over all of the experiments conducted. Out of the four attributes used, three are from the L*a*b* color space and one is from the L*u*v* color space; all are features computed using CCMs. Table III shows the confusion matrix obtained in this experiment, which demonstrates good performance with the fibrin and mixed classes, with accuracy up to 80%.

The KNN and decision tree classifiers provided the best performance using eight features,which were the attributes selected five or more times, with the correct classification rate of 73.6% and 71.5%, and AUC of 0.87 and 0.79, respectively. Out of the eight attributes that were selected five times or more, five are from the L*a*b* color space and three are from the L*u*v* color space; six of these features are based on CCMs and two
are texture features of individual components.

We can observe that in every case of highest performance of each classifier, only features from the L*a*b* and the L*u*v* color spaces were used, and most of them are features extracted from CCMs. Furthermore, these features were selected more often than features extracted from individual color components
The L*u*v* representation provides a uniform color space inwhich color differences correspond to differences as perceived by the human eye. The L*a*b* representation includes nonlinear transformations to emulate logarithmic characteristics of the human eye. Among the four color spaces used in this study,
the L*a*b* and L*u*v* spaces are designed to provide representations that facilitate analysis of color in the closest manner possible to human visual perception. In this study, results
of classification of ulcers based on texture analysis have been evaluated with reference to the results of visual analysis of the images by an MACF. The better performance of the texture features derived from the L*a*b* and L*u*v* spaces, as compared with the same derived from the RGB and HSI spaces, confirms that the L*a*b* and L*u*v* representations agree well with the human perceptual characteristics. Furthermore, the improved performance of the CCM features derived from the L*a*b* and L*u*v* spaces indicates that the correlation existing between the multiple channels of color representation carries useful information for texture analysis.

In summary, we can state that, based on the experiments conducted in this study, the best approach to the classification of color images of dermatological ulcers is the MLP classifier with the following features: homogeneity between the components a* and b*, contrast between the components a* and b*, entropy between a* and b*, and contrast between the components u*and v*.

Limitations exist in this study due to the small size of the database used, especially in the callous and necrotic tissue categories. Difficulties were encountered in applying the imaging protocol in a consistent manner. The images were acquired in a clinical environment and not in a research laboratory. In some cases, considerations related to the patient's mobility affected positioning and imaging of the ulcer. Such considerations also affected the distance and orientation of the camera, illumination of the ulcer, and composition of the image. Procedures need to be developed for color correction and normalization. It would be desirable to include procedures for comparative analysis of an ulcer region with reference to the color characteristics of the
surrounding normal skin of the patient. Further study is desired with a larger database of images, including longitudinal series of images of the same patients under treatment. Clinical interpretation of images of dermatological ulcers is based on visual analysis of the tissue composition as indicated by their color characteristics. This, however, is a subjective or qualitative approach that is affected by interobserver and in traobserver variability. Estimation of the fractional composition of an ulcer in terms of tissue types, such as granulation and fibrin, is nearly impossible via visual analysis. Analysis of the reliability of the labeling of ulcers by a dermatologist is beyond of the scope of the present study. We expect objective analysis of images of ulcers, as proposed in this study, to overcome some of the difficulties associated with visual analysis.

TABLE I FREQUENCY OF SELECTION OF EACH ATTRIBUTE FOR THE HSI, L*A*B*, L*U*V*, AND RGB COLOR SPACES

	HIS	L*a*b*	L*u*v*	RGB
Not selected	Mean in S	Contrast in b*; Skewness in b*; Kurtosis in b*	Correlation in v*	Homogeneity in R; Homogeneity in G; Local homogeneity in G;

				Contrast in B; Correlation in B; Local homogeneity between R and G; Entropy between G and B
Once	Homogeneity between H and S; Homogeneity in H; Homogeneity in S; Local homogeneity in S; Kurtosis in S; Mean in H	Correlation between a* and b*; Contrast in a*; Correlation in a*; Local homogeneity in b*; Skewness in a*; Mean in b*	Correlation in u*; Entropy in u*; Local homogeneity in v*; Mean in u*; Kurtosis in u*; Skewness in v*; Kurtosis in v*	Entropy in G; Entropy in B; Local homogeneity in B; Homogeneity between R and B; Contrast between R and B; Local homogeneity between G and B; Mean in G; Kurtosis in G; Mean in B
Twice	Contrast in H; Correlation in H; Entropy in H; Local homogeneity in H; Entropy in S; Standard deviation in S; Kurtosis in H;	Local homogeneity in a*; Standard deviation in a*; Kurtosis in a*; Standard deviation in b*	Correlation between u* and v*; Entropy between u* and v*; Homogeneity in u*; Contrast in u*; Local homogeneity in u*; Contrast	Contrast in R; Correlation in R; Homogeneity in B; Homogeneity between R and G; Entropy between R and G; Entropy between R and B; Homogeneity
			in v*; Standard deviation in u*	between G and B; Standard deviation in R; Kurtosis in R; Skewness in B; Kurtosis in B
Three times	Contrast between H and S; Correlation between H and S; Entropy between H and S; Contrast in S; Correlation in S; Skewness in S; Standard deviation in H; Skewness in H	Entropy in a*; Correlation in b*	Mean in v*; Standard deviation in v*	Correlation in R; Contrast in G; Correlation in G; Correlation between R and B; Local homogeneity between R and B; Contrast between G and B; Skewness in R; Skewness in G
Four times	Local homogeneity between H and S	Homogeneity in b*; Entropy in b*; Mean in b*	Local homogeneity between u* an v*; Homogeneity in v*; Skewness in u*	Local homogeneity in R; Contrast between R and G; Correlation between R and G; Correlation between G and B; Mean in R
Five times	None	Local homogeneity between a* and b*;	Homogeneity between u* and v*; Entropy	None

		Homogeneity in a*	in v*	
Six times	None	Contrast between a* and b*	None	None
Seven times	None	Homogeneity between a* and b*	None	None
Eight times	None	Entropy between a* and b*	Contrast between u* and v*	None

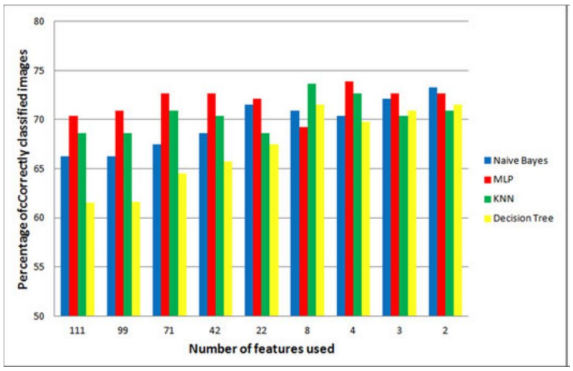

Fig. 3. Percentage of correctly classified images with each classifier using different thresholds on the frequency of selection of the attributes. The labels on the horizontal axis indicate the numbers of features in the various sets of features used, starting with all of the 111 features computed, the features selected once (99), twice (71), and so on to eight times (2).

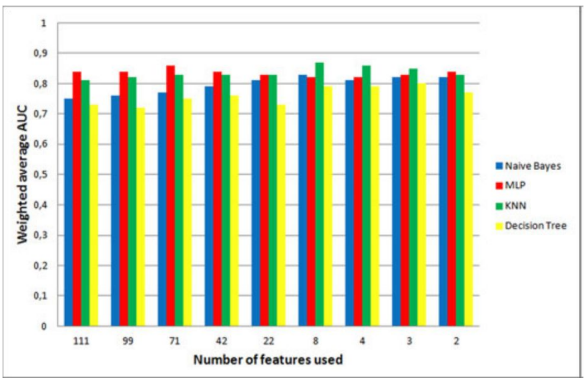

Fig. 4. Weighted average AUC for each classifier using different thresholds on the frequency of selection of the attributes. The labels on the horizontal axis indicate the numbers of features in the various sets of features used, starting with all of the 111 features computed, the features selected once (99), twice(71), and so on to eight times (2).

TABLE II CONFUSION MATRIX OF CLASSIFICATION USING ALL OF THE 111 EXTRACTED FEAT URES AND THE MLP

Real/ MLP	Granulation	Fibrin	Necrotic	Callous	Mixed	Total
Granulation	31	3	0	0	17	51
Fibrin	1	24	0	0	6	31
Necrotic	0	0	0	0	3	3
Callous	0	0	0	2	1	3
Mixed	14	2	2	2	64	84

The table shows, in each row, the real image class, and in each column, the MLP classification.

IV. CONCLUSION

The evaluation of tissue composition provides key informationfor monitoring the response to treatment of patients with chronic ulcers. Quantitative measures characterizing tissue composition can make significant contributions to the evaluation of the healing process. In this study, we have demonstrated the potential use of methods of digital image processing and pattern recognition based on artificial intelligence to facilitate the characterization of tissue composition of skin ulcers. Statistical measures derived from CCMs of the L*a*b* and L*u*v* color components provided better classification performance than the same measures derived from the the RGB and HSI components. Out of the four classifiers tested, the MLP provided the best overall performance.We believe that objective analysis of color images of skin ulcers using the proposed methods can overcome some of the limitations of visual analysis and lead to the development of improved protocols for the treatment and monitoring of chronic dermatological lesions. Furthermore, such approaches can assist in the development of optimized and personalized therapy for each patient.

REFERENCES

[1] M. J. Callam, C. V. Ruckley, D. R. Harper, and J. J. Dale, “Chronic ulceration of the leg: Extent of the problem and provision of care,” *Brit. Med.J. (Clin. Res. ed.)*, vol. 290, no. 6485, pp. 1855–1856, 1985.

[2] S. Herrick, P. Sloan, M. McGurk, L. Freak, C. McCollum, and M. Ferguson, “Sequential changes in histologic pattern and extracellular matrix deposition during the healing of chronic venous ulcers,” *Amer. J. Pathol.*, vol. 141, no. 5, pp. 1085–1095, 1992.

[3] M. Witte and A. Barbul, "General principles of wound healing," *Surg. Clin. North Amer*., vol. 77, no. 3, pp. 509–528, 1997.

[4] K. Burnand, I. Whimster, and A. Naidoo, "Pericapillary fibrin in the ulcerbearing skin of the leg: The cause of lipodermatosclerosis and venous ulceration," *Brit. Med. J. (Clin. Res. ed.)*, vol. 285, no. 6348, pp. 1071–1072, 1982.

[5] M. Rezvani, M. Robbins, J. Hopewell, and E. Whitehouse, "Modification of late dermal necrosis in the pig by treatment with multi-wavelength light," *Brit. J. Radiol.*, vol. 66, no. 782, pp. 145–149, 1993.

[6] T. Pavicic and H. Korting, "Xerosis and callus formation as a key to the diabetic foot syndrome: Dermatologic view of the problem and its management," *J. Deutschen Dermatolog. Gesellschaft*, vol. 4, no. 11,
pp. 935–941, 2006.

[7] H. Murray, M. Young, S. Hollis, and A. Boulton, "The association between callus formation, high pressures and neuropathy in diabetic foot ulceration," *Diabet. Med.*, vol. 13, no. 11, pp. 979–982, 1996.

[8] I. Maglogiannis, S. Pavlopoulos, and D. Koutsouris, "An integrated computer supported acquisition, handling, and characterization system for pigmented
skin lesions in dermatological images," *IEEE Trans. Inf. Technol. Biomed.*, vol. 9, no. 1, pp. 86–98, Mar. 2005.

[9] H.Wannous, S. Treuillet, andY. Lucas, "Robust tissue classification for reproducible wound assessment in telemedicine environments," *J. Electron.Imag.*, vol. 19, p. 023002, 2010.

[10] H. Oduncu, A. Hoppe, M. Clark, R. Williams, and K. Harding, "Analysis of skin wound images using digital color image processing: A preliminary communication," *Int. J. Low Extreme Wounds*, vol. 3, no. 3, pp. 151–156,2004.

[11] A. Tarallo, A. Gonzaga, and M. Frade, "Artificial neural networks applied to the segmentation and classification of digital images of cutaneous ulcers," in *Proc. IEEE 7th Int. Conf. Bioinformat. Bioeng.*, 2007, pp. 1–1.

[12] S. M. Pereira, M. A. C. Frade, R. M. Rangayyan, and P. M.de Azevedo Marques. (2011). Classification of dermatological ulcers based on tissue composition and color texture features. in *Proc. 4th Int. Symp. Appl. Sci. Biomed. Commun. Technol.*, ser. ISABEL 2011. Barcelona, Spain: ACM, [Online]. pp. 68:1–68:6. Available: http://doi.acm.org/10.1145/2093698.2093766

[13] E. Dorileo, M. Frade, A. Roselino, R. Rangayyan, and P. Azevedo- Marques, "Color image processing and content-based image retrieval techniques for the analysis of dermatological lesions," in *Proc. 30th Annu. Int. Conf. IEEE Eng. Med. Biol. Soc.*. Vancouver, BC, Canada, Aug. 2008, pp. 1230–1233.

[14] R. Rangayyan, B. Acha, and C. Serrano. (2011). *Color Image Processing With Biomedical Applications*, ser. Press monograph 206. SPIE. [Online]. Available: http://books.google.co.in/books?id=a9CzuAAACAAJ

[15] R. Gonzalez and R. Woods, *Digital Image Processing*, 3rd ed. Englewood Cliffs, NJ: Pearson Prentice Hall, 2008.

[16] R. Haralick, K. Shanmugam, and I. Dinstein, "Textural features for image classification," *IEEE Trans. Syst., Man, Cybern.*, vol. TSMC-3, no. 6,pp. 610–621, Nov. 1973.

[17] R. W. Conners and C. A. Harlow, "A theoretical comparison of texture algorithms," *IEEE Trans. Pattern Anal. Mach. Intell.*, vol. PAMI-2, no. 3, pp. 204–222, May 1980.

[18] V. Arvis, C. Debain, M. Berducat, and A. Benassi, "Generalization of the cooccurrence matrix for colour images: Application to colour texture classification," *Image Anal. Stereol.*, vol. 23, no. 1, pp. 63–72, 2004.

[19] R. Kohavi, "A study of cross-validation and bootstrap for accuracy estimation and model selection," in *Proc. Int. Joint Conf. Artif. Intell.*, 1995, vol. 14, pp. 1137–1145.

[20] T. M. Mitchell, *Machine Learning*, 1st ed. New York: McGraw-Hill, Inc., 1997.

[21] A. L. Blum and P. Langley. (1997, Dec.). Selection of relevant features and examples in machine learning. *Artif. intell.*, [Online]. vol. 971–2, pp. 245– 271, Available:http://dx.doi.org/10.1016/S00043702(97)00063-5

[22] M. Hall, E. Frank, G. Holmes, B. Pfahringer, P. Reutemann, and I.Witten, "The Weka data mining software: An update," *ACM Spec. Inter. Group Knowl. Disc. Data Mining (SIGKDD) Explorat. Newslett.*, vol. 11, no. 1,pp. 10–18, 2009.

[23] P. Domingos andM. J. Pazzani, "On the optimality of the simple Bayesian classifier under zero-one loss," *Mach. Learn.*, vol. 29, no. 2, pp. 103–130,1997.

[24] N. Vaziri, A. Hojabri, A. Erfani, M. Monsefi, and B. Nilforooshan, "Critical heat flux prediction by using radial basis function and multilayer perceptron neural networks: A comparison study," *Nuclear Eng. Des.*,vol. 237, no. 4, pp. 377–385, 2007.

[25] J. Quinlan, "Decision trees and decision-making," *IEEE Trans. Syst.,Man, Cybern.*, vol. 20, no. 2, pp. 339–346, Mar./Apr. 1990.